



HAL
open science

Quantum and classical molecular dynamics for H atom scattering from graphene

Lei Shi, Markus Schröder, Hans-Dieter Meyer, Daniel Peláez, Alec M Wodtke, Kai Golibrzuch, Anna-Maria Schönemann, Alexander Kandratsenka, Fabien Gatti

► **To cite this version:**

Lei Shi, Markus Schröder, Hans-Dieter Meyer, Daniel Peláez, Alec M Wodtke, et al.. Quantum and classical molecular dynamics for H atom scattering from graphene. *Journal of Chemical Physics*, 2023, 159 (19), pp.194102. 10.1063/5.0176655 . hal-04304720

HAL Id: hal-04304720

<https://hal.science/hal-04304720>

Submitted on 24 Nov 2023

HAL is a multi-disciplinary open access archive for the deposit and dissemination of scientific research documents, whether they are published or not. The documents may come from teaching and research institutions in France or abroad, or from public or private research centers.

L'archive ouverte pluridisciplinaire **HAL**, est destinée au dépôt et à la diffusion de documents scientifiques de niveau recherche, publiés ou non, émanant des établissements d'enseignement et de recherche français ou étrangers, des laboratoires publics ou privés.

Quantum and classical molecular dynamics for H atom scattering from graphene

Lei Shi,¹ Markus Schröder,² Hans-Dieter Meyer,² Daniel Peláez,¹ Alec M. Wodtke,^{3, a)}
Kai Golibrzuch,³ Anna-Maria Schönemann,^{3, a)} Alexander Kandratsenka,³ and Fabien
Gatti ^{*1, b)}

¹⁾ *Université Paris-Saclay, CNRS, Institut des Sciences Moléculaires d'Orsay UMR
8214, 91405, Orsay, France.*

²⁾ *Theoretische Chemie, Physikalisch-Chemisches Institut,
Universität Heidelberg, Im Neuenheimer Feld 229, 69120, Heidelberg,
Germany.*

³⁾ *Dept. of Dynamics at Surfaces, Max Planck Institute for Multidisciplinary Sciences,
am Faßberg 11, 37077 Göttingen, Germany.*

(Dated: 24 November 2023)

^{a)}Institute for Physical Chemistry, Georg-August University of Göttingen, Tammannstraße 6, 37077
Göttingen, Germany.

^{b)}Electronic mail: fabien.gatti@universite-paris-saclay.fr

This work presents systematic comparisons between classical molecular dynamics (cMD) and quantum dynamics (QD) simulations of 15-dimensional and 75-dimensional models in their description of H atom scattering from graphene. We use an experimentally validated full-dimensional neural network potential energy surface (NN-PES) of a hydrogen atom interacting with a large cell of graphene containing 24 carbon atoms. For the quantum dynamics simulations, we apply Monte Carlo Canonical Polyadic Decomposition (MCCPD) to transform the original PES into a Sum of Products (SOP) form and use the Multi-layer Multi-configuration Time-dependent Hartree (ML-MCTDH) method to simulate the quantum scattering of a hydrogen or deuterium atom with an initial kinetic energy of 1.96 eV or 0.96 eV and incident angle of 0° , i.e. perpendicular to the graphene surface. The cMD and QD initial conditions have been carefully chosen in order to be as close as possible. Our results show little differences between the cMD and QD simulations when the incident energy of the H atom is equal to 1.96 eV. However, a large difference in sticking probability is observed when the incident energy of the H atom is equal to 0.96 eV, indicating the predominance of quantum effects. To the best of our knowledge, our work provides the first benchmark of quantum against classical simulations for a system of this size with a realistic PES. Additionally, new projectors are implemented in the Heidelberg MCTDH package for the calculation of the atom scattering energy transfer distribution as a function of the outgoing angles.

I. INTRODUCTION

Graphene is a bi-dimensional crystal material first defined by P. R. Wallace in 1947¹ and isolated for the first time in 2004 by K. S. Novoselov and A. K. Geim². Graphene has unique electronic, magnetic, and chemical properties that make it a promising material for various applications such as electronics, energy storage, and sensing³⁻⁶. Due to its exceptional properties, Graphene is the subject of extensive research in various fields of science and technology. Besides, chemical modification of graphene can introduce new properties and, in turn, lead to potential applications⁷, for example, hydrogenated graphene can create a local band gap and make it possible to produce a graphene semiconductor⁸. In addition, the hydrogenation of graphene is also a promising model system for the study of mechanisms of vibrational redistribution reactions⁹.

The scattering of H atoms from the graphene surface is an active area of research¹⁰. The study of the interaction between hydrogen atoms and graphene can provide essential insights into the fundamental mechanisms of the formation of the C-H chemical bond and also into hydrogen storage¹¹. The experiments on hydrogen scattering reported recently⁹ provide a ground for understanding the adsorption of hydrogen atoms on the graphene surface as well as the mechanisms of the energy transfer at scattering and vibrational redistribution reactions. In the experiment, a beam of H atoms with narrow incidence energy distribution and well-defined incidence angle was scattered from a graphene surface, and the kinetic energy of the outgoing H atoms was measured using the Rydberg atom time-of-flight (TOF) techniques.

One of the most crucial components in the theoretical modelling of the atomic scattering from surfaces is a potential energy surface (PES), accurate enough to correctly describe chemically relevant properties (energy barriers, adsorption energies etc.). A full-dimensional neural network PES (NN-PES) for a H atom interacting with a graphene was constructed recently¹² using machine learning methods adapted to large condensed systems¹³. The NN-PES was trained on a set of over 75 000 configurations calculated with the GGA-DFT PBE functional for a hydrogen atom and 24 carbon atoms representing graphene surface. This resulted in a fit with root mean standard error of $0.6 \text{ meV}/\text{atom}$. The classical molecular dynamics (cMD) simulations of H scattering from graphene produced energy loss spectra and angular distributions of scattered H atoms in good agreement with the experimental data¹².

While the cMD was largely successful in reproducing the experiment, H atom scattering from graphene is fundamentally a quantum system¹⁴, due both to the light mass of the H atom and the single-layer of C atoms. Interestingly, ring polymer molecular dynamics (RPMD) simulations addressing this issue showed little difference to cMD simulations¹⁴. Unfortunately, due to the approximations used in its derivation, it is not clear whether RPMD is suitable for describing non-equilibrium scattering processes occurring on the short-time (dozens to hundreds fs) scale. Quantum dynamics (QD) simulations are thus needed both to test the reliability of RPMD simulations and to rigorously reveal quantum effects in the scattering process.

Quantum dynamics is computationally challenging for such a high-dimensional system (24 graphene C atoms and a H atom add up to 75 DoFs), since the computational time and memory requirements for calculations increase exponentially with the dimensionality of the system. This is due to the fact that the wave function describing a quantum state of the system has to be represented in a high-dimensional configuration space, and the number of basis set functions to describe the system also increases exponentially with the dimensionality. To overcome these difficulties, we use multi-configuration time-dependent Hartree (MCTDH)^{15–21} approach to solve the time-dependent Schrödinger equation much faster and with much smaller memory demands than conventional methods. This method is extremely suitable for systems with the large number of degrees of freedom (DoFs). Unfortunately, to achieve the aforementioned effectiveness, it is necessary to represent the PES in a sum-of-products (SOP) form. This can be achieved, for example, by refitting the existing PES using a tensor decomposition method^{22–26}. That can be rather difficult because of the large number of parameters to be determined and the high computational cost associated with the process. There exists an alternative to refitting, the correlation discrete variable representation method^{27–29} by U. Manthe, which, however, requires very many potential energy evaluations during propagation, so we do not consider it here.

In this work, we perform 75-dimensional QD simulations of the H scattering from graphene using as input the experimentally validated NN-PES¹². The recently developed methods: Monte Carlo Canonical Polyadic Decomposition³⁰ (MCCPD) for PES transformation, and the advanced multi-layer MCTDH^{31–33} propagator make that task quite realistic. Besides, we assess these simulations with QD simulations for the system with reduced dimensionality. Initially, we have chosen to fix the positions of 20 of the 24 carbon atoms at

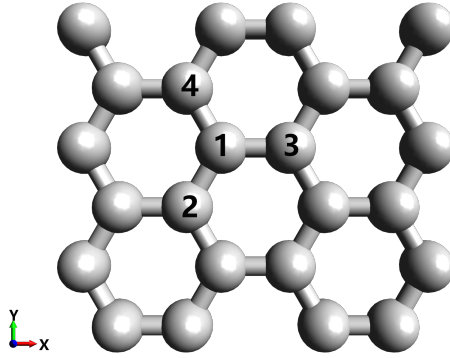


FIG. 1. Graphene surface simulation cell: the impact site is labelled by 1; C-atoms forming the first shell around the 1st atom are labelled by 2, 3, and 4. The surface is in the X,Y plane, the Z direction is perpendicular to the surface.

their equilibrium geometry and allow the remaining 4 C-atoms and the H-atom to move. This reduces the dimensionality of the system from 75D to 15D, making it computationally much more robust and feasible. Figure 1 shows the structure of the graphene surface, where an H-atom impact site is labelled by 1, and C-atoms forming the first shell around the central C-atom are labelled by 2, 3, and 4. The labelled C-atoms are allowed to move in the model with reduced dimensions.

It is important to keep in mind that the model with the reduced number of dimensions introduced above may not capture all the details of the full-dimensional system and thus can fail to reproduce the experimental results. For example, in the reduced model, the incident H atom hits a C-atom 1 while the scattering from the other sites is not taken into account to prevent contributions from the fixed part of the graphene into the scattering amplitudes. So, the simulations in the reduced dimensions cannot substitute the full-dimensional quantum simulations. The latter are hence used to assess the relevance of the quantum-mechanical effects by comparison to the cMD simulations.

As main conclusion, we find that the results of QD simulations compare well with experimental angular and energy scattering distributions. The quantum effects display themselves in sticking probability even at incidence energies as high as 0.96 eV .

II. CLASSICAL MD AND QD SIMULATIONS DETAILS

The QD simulations were performed using the *Heidelberg MCTDH Package*³⁴, the cMD simulations are realized by *md.tian2*³⁵. The initial conditions were chosen to reproduce the incidence energy value of 1.96 eV and the normal incidence angle for the H and D atoms, since at these conditions the deviation of the cMD simulations from experimental results is most pronounced.

In the classical MD simulations, the projectile has a sharp incidence kinetic energy and incidence angle. In case of QD, we have to deal with the corresponding distributions defined by the initial wavefunction. It is important, therefore, to bring the initial conditions for the classical and quantum simulations as close as possible to each other. In the following we introduce the methods that we used to extract the same information from both simulations.

A. Coordinates

The cMD simulations were done using Cartesian coordinates. However, for QD simulations, we opted to use normal mode coordinates for the graphene surface and Cartesian coordinates for the hydrogen atom. This choice was motivated by the fact that the potential energy of the graphene surface is approximately harmonic at room temperature, and the use of normal mode coordinates allows us to decouple the DoFs of the graphene in a good approximation. This approach facilitates the convergence of our calculations and leads to more efficient simulations.

The transformation from Cartesian \mathbf{x} to (mass and frequency weighted) normal \mathbf{q} coordinates (cf. Ref. 36),

$$q_\alpha = \omega_\alpha^{1/2} \sum_{n=1}^f (x_n - x_n^{(\text{eq})}) L_{n\alpha}, \quad (1)$$

is determined by the matrix \mathbf{L} diagonalizing the mass-weighted Hessian matrix \mathbf{GF}_{eq} :

$$\mathbf{GF}_{\text{eq}}\mathbf{L} = \mathbf{L}\boldsymbol{\omega}^2. \quad (2)$$

Here, $G_{kn} = 1/\sqrt{m_k m_n}$ is the mass matrix, $F_{\text{eq},kn} = \left. \frac{\partial^2 V}{\partial x_k \partial x_n} \right|_{\mathbf{x}=\mathbf{x}_{\text{eq}}}$ is the Hessian matrix for the potential V calculated at equilibrium geometry \mathbf{x}_{eq} when the H atom is far from the surface, $\boldsymbol{\omega}^2$ is the diagonal matrix of eigenvalues of the Hessian, which are squares of the frequencies of the normal modes.

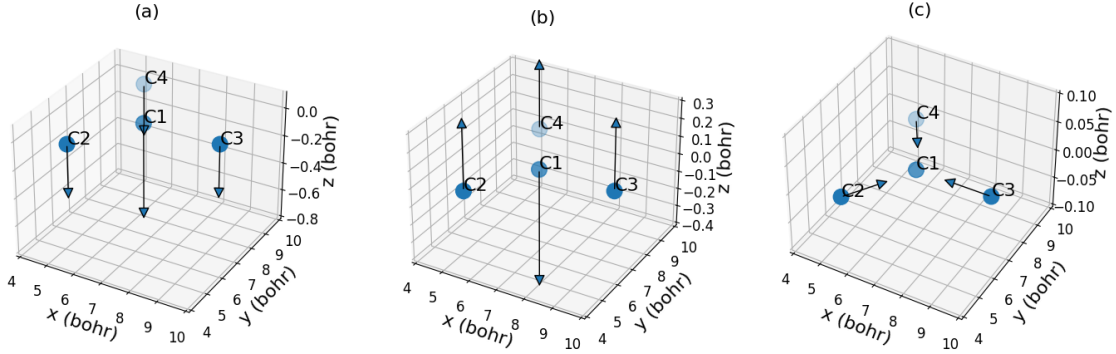


FIG. 2. Three most important normal modes participating in the energy transfer during the H atom collision with graphene: mode q_1 (a), mode q_4 (b), and mode q_{10} (c).

In the case of the reduced 15-dimensional system with four movable C atoms, the normal modes have been computed for these four C atoms, while all other carbon atoms, not shown in Figure 1, are fixed at their equilibrium position at 0 K and the H atom is far from the surface. Consequently, there are a total of twelve normal modes used to describe the motion of the graphene slab. Three of them are of particular importance in the MD simulations of scattering, which will be discussed in detail in the next Section: modes q_1 (Figure 2a) and q_4 (Figure 2b) are transverse modes incorporating the motion of the central C atom in z direction and participating in the formation of a C-H chemical bond; q_{10} (Figure 2c) is the breathing vibrational mode for the first shell C atoms.

In the case of the full-dimensional system, all 24 C atoms can move. The normal modes are determined by treating the graphene cell as periodic and the H atom is far from the surface, resulting in a total of 72 normal modes for the graphene surface. However, due to the periodic nature of the PES for the graphene cell, 3 translation normal modes exhibit nearly zero or negative frequencies. These three modes should be removed, resulting in a final count of sixty-nine normal modes necessary to characterize the behavior of the graphene surface.

B. PES refitting

In order to put the high-dimensional NN-PES into the sum of products (SOP) form necessary for MCTDH propagation, we used the MCCPD³⁰ method, which is briefly described below.

The PES $V(q_1, q_2, \dots, q_f)$ is approximated by a canonical polyadic decomposition (CPD) form:

$$V^{\text{CPD}}(q_1, q_2, \dots, q_f) = \sum_{r=1}^R c_r \prod_{\kappa=1}^f v_{\kappa}^r(q_{\kappa}), \quad (3)$$

or in the grid-representation after discretization of the coordinates \mathbf{q} :

$$V_{i_1, i_2, \dots, i_f}^{\text{CPD}} = \sum_{r=1}^R c_r \prod_{\kappa=1}^f v_{\kappa, i_{\kappa}}^r, \quad (4)$$

where index i_{κ} numbers discretization points of the coordinate q_{κ} , v_{κ}^r are basis functions with expansion coefficient c_r , and R is the expansion order (the rank of the decomposition). It should be noted here that, in general, no restrictions are enforced on the orthogonality of the basis functions v_{κ}^r and normalization can be arbitrary (coefficient c_r could be absorbed into any of the basis functions). However, the basis functions are often restricted to be normalized to reduce ambiguity, so we adopted this restriction in this work.

Introducing the composite index $I = \{i_1, \dots, i_f\}$ and the composite single-hole index $I^{\kappa} = \{i_1, i_2, \dots, i_{\kappa-1}, i_{\kappa+1}, \dots, i_f\}$, the decomposition is obtained by optimization of the weighted \mathcal{L}^2 difference between the fitting potential V_I^{CPD} from Eq. (4) and the exact potential V_I . This can be cast into minimizing the functional

$$J = \sum_I W_I (V_I - V_I^{\text{CPD}})^2 + \epsilon \sum_{I,r} W_I c_r^2 \left(\prod_{\kappa=1}^f v_{\kappa, i_{\kappa}}^r \right)^2, \quad (5)$$

where W is a positive weight function depending on all coordinates \mathbf{q} , which imposes more weights on the regions the PES that should be fitted with elevated accuracy (for instance, low energy regions where the wavefunction resides). The second term in the r.h.s of Eq. (5) proportional to ϵ serves as a regularization with ϵ being a small parameter which is set to the square root of machine precision, i.e., $\epsilon \approx 1 \cdot 10^{-8}$. It preserves the linear independence of the basis functions v_{κ}^r during the optimization process.

A functional derivative of the functional J defined by Eq. (5) with respect to basis functions $c_r v_{\kappa, i_{\kappa}}^r$ produces a system of linear equations which, in principle, can be solved. In practice, solving these equations is simplified by replacing the weight function W with a factorized approximation for every coordinate q_{κ} :

$$W_I \approx w_{i_{\kappa}}^{\kappa} W_{I^{\kappa}}, \quad (6)$$

and considering a set of the functionals J^κ instead of J :

$$J^\kappa = \sum_I w_{i_\kappa}^\kappa W_{I^\kappa}^\kappa (V_I - V_I^{\text{CPD}}) + \epsilon \sum_{I,r} w_{i_\kappa}^\kappa W_{I^\kappa}^\kappa \left(\prod_{\kappa=1}^f v_{\kappa, i_\kappa}^r \right)^2. \quad (7)$$

Then calculating the functional derivative of Eq. (7) with respect to $c_r v_\kappa^r$ and setting them to zero leads to a system of linear equations for $c_r v_\kappa^r$:

$$\sum_{r'} S_{r,r'}^\kappa c_{r'} v_{\kappa, i_\kappa}^{r'} = B_{r, i_\kappa}^\kappa \quad (8)$$

with

$$S_{r,r'}^\kappa = \sum_{I^\kappa} W_{I^\kappa}^\kappa \left[\prod_{\kappa' \neq \kappa} v_{\kappa', i_{\kappa'}}^r v_{\kappa', i_{\kappa'}}^{r'} (1 + \epsilon \delta_{r,r'}) \right], \quad (9)$$

$$B_{r, i_\kappa}^\kappa = \sum_{I^\kappa} W_{I^\kappa}^\kappa V_I \prod_{\kappa' \neq \kappa} v_{\kappa', i_{\kappa'}}^r. \quad (10)$$

Note that $w_{i_\kappa}^\kappa$ drops out and $W_{I^\kappa}^\kappa$ is conveniently defined as $W_{I^\kappa}^\kappa = \sum_{i_\kappa} W_I$. Standard linear algebra tools can now be used to solve Eq. (8). Note, that Eqs. (9) and (10) imply that the solution for mode κ depends on all other modes. So, one has to start with an initial guess for the CPD decomposition and to get solution for all modes consecutively, then to update the CPD tensor after solving Eq. (8), and finally, once all modes are updated, to iterate until either a convergence criterion is met or a maximum number of iterations is reached. This procedure is known as the alternating least squares (ALS) algorithm. A very efficient way to accelerate convergence is to start with a small rank R , perform a number of iterations and subsequently increase R , where the new coefficients c_r are set to zero and the new basis functions v_κ^r are filled with random numbers.

The ALS iterations defined by Eqs. (8–10) are computationally feasible only when the number of points I to be processed is not larger than 10^9 – 10^{10} , so that the matrices \mathbf{S}^κ and \mathbf{B}^κ can actually be computed. To tackle the system considered in this work the total number of points has to be of order of 10^{20} , so we evaluate the sums in Eqs. (9) and (10) using a Monte-Carlo sampling with the distribution functions defined by W^κ weights³⁰. The sampling strategy proved to affect strongly the accuracy of the fit. For example, Metropolis sampling proved to lead to satisfying results^{30,37}. Here, the distribution function is proportional to $\exp(-\beta V)$ with β being a positive parameter and roughly resembles the ground state wavefunction if, in the harmonic approximation $\beta = 1/\hbar\omega$, and $V = m\omega^2 x^2/2$ with

m , ω being the mass and frequency of the harmonic oscillator, respectively. It emphasizes low energy regions and covers the area where the wavefunction mostly resides. However, the sampling distribution is derived only from the potential part of the total Hamiltonian and neglects the influence of the kinetic energy operator, which makes it not accurate enough. Furthermore, for multi-dimensional surfaces usually each coordinate is approximated by a different harmonic oscillator such that one needs to find a single parameter β that establishes a compromise between the various harmonic frequencies.

Obviously, the sampling method described above is not well suited for systems with very different fundamental frequencies - and therefore not used in this work. In order to avoid the above deficiency and obtain a sampling distribution proportional to the ground state wavefunction, we performed two diffusion Monte-Carlo (DMC)³⁸ simulations. From them we obtained the vibrational ground state distributions for the graphene not interacting with a projectile (H atom is far away from the surface) and for the graphene with the H atom close to it. The sampling points obtained from both calculations were subsequently merged into a single set and each sampling point was mapped onto the nearest Discrete Variable Representation (DVR) point.

In total 250 291 sampling points were calculated in the regions with potential energy varying from the minimum of the PES to about 3.5 eV, since the energy accessible in the dynamic simulations was smaller than 3 eV. We began the ALS optimization with a rank $R = 128$, increasing it in every 10 iterations by 64 until the value of $R = 512$ was reached. Figure 3 shows the improvement of the fit quality with ALS-iterations given by the root mean square error (RMSE) of the model's predictions. The final RMSE is 74.9 cm⁻¹.

Then we generated 401 758 sampling points from the DMC calculations to test and validate the refitted PES. The quality of refitting is shown in figure 4.

C. Initial conditions

Classically, the positions and momenta of particles can be defined precisely, while in the QD calculation, the state of the system is described by the wave function. This fundamental difference makes the comparison of results of cMD and QD simulations not straightforward. Thus, it is important to set the initial conditions for the classical and quantum simulations in such a way to be able to refer to them as similar.

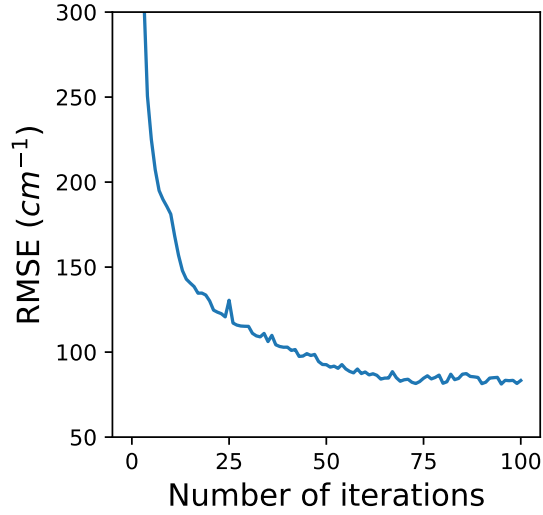


FIG. 3. The RMSE dependance on the number of iteration during the CPD optimization.

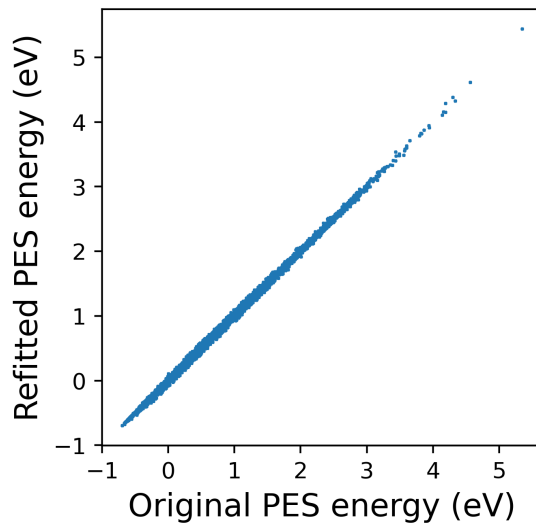


FIG. 4. The validation of the refitted PES calculated by the MCCPD calculation.

In case of the quantum dynamic simulations, we define the initial state of graphene as the ground state constructed as a solution of the Schrödinger time-dependent equation for a negative imaginary time propagation³⁹:

$$\Psi(\mathbf{x}, t) = \sum c_n \varphi_n(\mathbf{x}) e^{-E_n t}, \quad (11)$$

where $\varphi_n(\mathbf{x})$ is the n th eigenstate and E_n is the corresponding eigenenergy and $\hbar = 1$ is assumed. Because of the exponential term in Eq.(11), the eigenstates with higher energy will vanish faster during the relaxation, and the system converges towards the ground state with

increasing propagation time. Using this method, we found the ground state energy value of 0.710 eV for the system with the reduced dimensions (4 movable C atoms). On the other hand, the corresponding vibrational ground state energy in the harmonic approximation $\sum 0.5\omega_i = 0.698$ eV, where frequencies were calculated in the normal mode section. The values agree well, which makes it reasonable to describe a free-standing graphene surface within harmonic approximation.

The initial wavepacket for an H atom has to move along the normal to the surface with the kinetic energy expectation value of 1.96 eV or 0.96 eV, and the position distribution of the incident H atom has to be narrow. To this end, we used a Gaussian wavepacket for the H atom in z direction and complex Gaussian wavepackets for the in-plane DoFs⁴⁰

$$\Psi(x, t = 0) = A \exp [-(a + ib)(x - x_0)^2] . \quad (12)$$

to mimic the initial state of the H atom. The reason for using complex Gaussians is to prevent the wavepacket from the broadening during the propagation in the interaction-free region since a complex parameterized Gaussian wavefunction first narrows and then spreads, as can be seen from its variance dependence on time⁴⁰

$$\sigma(t) = \sqrt{\frac{a^2 + [\frac{2t}{m}(a^2 + b^2) - b]^2}{4a(a^2 + b^2)}} . \quad (13)$$

where m is the mass of the atom and $\hbar = 1$ is assumed. By varying the parameter b entering Eqs. (12) and (13) one can define the incident wavepacket to have the minimal width at the turning point, thus that an H atom 'hits' graphene at the well-defined site (C-atom labeled 1 in Figure 1). Here x stands for the X or Y coordinate, respectively, of the H-atom. The variance of the Gaussian function for the H-atom or D-atom in the X or Y direction is around 0.37 Bohr when hitting the graphene surface. The wave function is, thus, well localized to the attacked C-atom as shown in figure 5.

D. ML-MCTDH

In the MCTDH method, the molecular wavefunction is written as the SOP of orthonormal time-dependent single particle functions (SPFs) of logical coordinates Q_1, Q_2, \dots, Q_p :

$$\Psi(Q_1, \dots, Q_p, t) = \sum_{i_1=1}^{n_1} \cdots \sum_{i_p=1}^{n_p} A_{i_1, \dots, i_p}^1(t) \varphi_{i_1}^{1:1}(Q_1, t) \cdots \varphi_{i_p}^{1:p}(Q_p, t) \quad (14)$$

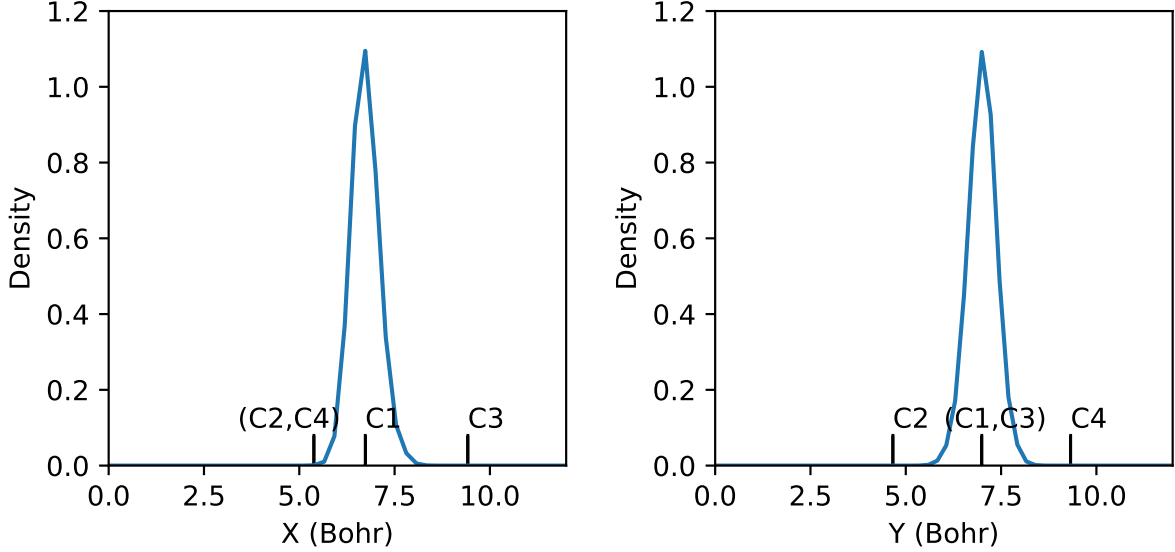


FIG. 5. Reduced density of H-atom wave function in the X and Y direction when hitting the surface. The coordinates of 4 numbered C atoms are indicated.

with SPFs defined as a linear combination of the primitive time-independent basis, for example,

$$\varphi_m^{1;\kappa}(Q_\kappa, t) = \sum_{j_1, \dots, j_d} A_{m, j_1, \dots, j_d}^{2;\kappa}(t) \chi_{j_1}^{\kappa, 1}(q_m^1) \cdots \chi_{j_d}^{\kappa, d}(q_m^d). \quad (15)$$

Here n_p is the number of SPFs used for the p th combined mode, d DoFs are combined to form the m th logical coordinate, $Q_m = (q_m^1, \dots, q_m^d)$. The logical coordinates are used to treat the correlation between the combined DoFs already on the SPF level, which improves the convergence of the calculation.

The type and the number of the primitive basis functions $\chi_{j_d}^{\kappa, d}(q_m^d)$ should be chosen carefully in order to adapt to the system and to converge the calculation. Table I lists the primitive basis used in the 15D QD simulation. We used a Fast Fourier Transform method (FFT) for Z coordinate of the H atom because the domain of this DoF is very large and so is the number of grid points needed, and a FFT accelerates a calculation for large grid sizes. For convenience, we also used a FFT for the in-plane H atom coordinates (see Eq. (20) below). For the normal modes of graphene, we used the harmonic oscillator (HO) DVR to optimally adapt to the system. The frequency and mass used for HO basis function in Table I are equal to 1.0, because the normal modes calculated with the mentioned method are dimensionless, the mass and frequency are included into the coordinates. It's important

TABLE I. The parameters for the definition of primitive basis functions. The second column indicates the kind of DVR, the third column gives the number of grid points, further parameters give more details about the DVR. In the case of FFT, they correspond to the coordinates of the first (P1) and last (P2) grid points and if it is periodic, it is written in the column (P3). In the case of HO, they correspond to the equilibrium position (P1), frequency (P2) and mass (P3) of harmonic oscillator basis functions.

DoF	Type	Grid size	P1	P2	P3
X	FFT	60	0.0	16.152614301	periodic
Y	FFT	60	0.0	13.988573798	periodic
Z	FFT	144	0.5	12.0	
q_1	HO	35	0.0	1.0	1.0
q_2	HO	13	0.0	1.0	1.0
q_3	HO	13	0.0	1.0	1.0
q_4	HO	30	0.0	1.0	1.0
q_5	HO	13	0.0	1.0	1.0
q_6	HO	13	0.0	1.0	1.0
q_7	HO	13	0.0	1.0	1.0
q_8	HO	13	0.0	1.0	1.0
q_9	HO	13	0.0	1.0	1.0
q_{10}	HO	23	0.0	1.0	1.0
q_{11}	HO	13	0.0	1.0	1.0
q_{12}	HO	13	0.0	1.0	1.0

to note that the normal modes of graphene were calculated under when the H atom being far from the surface. However, when the hydrogen atom approaches, it strongly alters the harmonic behavior of the graphene structure, rendering the initially calculated normal modes less optimal for the system. Consequently, more primitive basis functions are required to achieve a converged calculation. This explains the larger number of basis functions necessary for q_1 , q_4 , and q_{10} , as they exhibit a higher degree of correlation with the hydrogen atom.

Even for the reduced 15D system, the MCTDH calculations are still computationally very expensive. The Multi-Layer (ML) formulation of MCTDH helps to decrease the com-

putational costs. Here, instead of directly expanding the SPFs in terms of the primitive basis, as in Eq. (15), several layers of the expansion are introduced. For more details see Refs. 31–33. The structure of a ML-wavefunction is conveniently visualized by an ML tree shown in Figure 6. The wavefunction in ML-MCTDH is more compact, but it is challenging to find the optimal structure of the multi-layer tree to minimize the computation time and the convergence of calculations. When constructing the ML tree we followed several guiding lines: (i) strongly coupled DoFs were combined as early as possible; (ii) the population of the last time-dependent function for each node should be smaller than 10^{-3} to achieve good convergence of calculations.

Table II demonstrates that the last time-dependent functions for all nodes in the H atom scattering match the latter condition. We found that the structure of the ML tree displayed in Figure 6 is close to the optimum, so we used it to perform simulations of the H atom scattering from graphene.

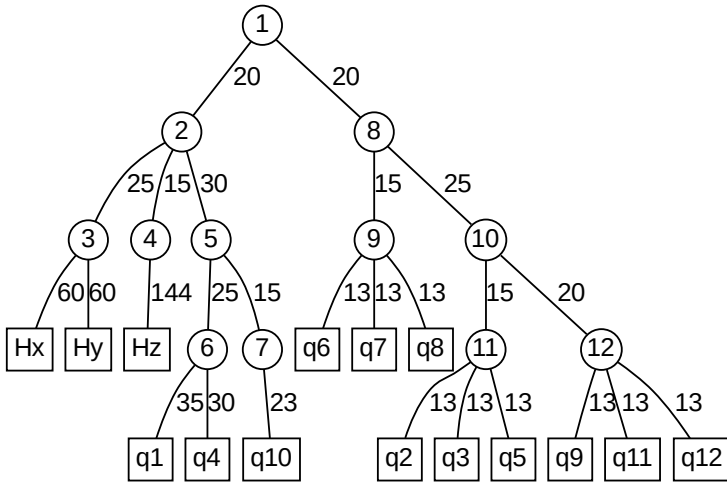


FIG. 6. ML tree structure for 15D simulation. Squares represent primitive basis functions, the circles—also called nodes—stand for time dependent A-tensors, and the numbers on the edges are the number of functions used

Layer	Node	Mode	Maximum population
0	1	1	5.457E-04
0	1	2	5.457E-04
1	2	1	2.106E-04
1	2	2	1.815E-05
1	2	3	1.799E-04
2	5	1	3.278E-05
2	5	2	4.190E-07
1	8	1	1.084E-05
1	8	2	6.700E-05
2	10	1	2.133E-05
2	10	2	3.455E-06

TABLE II. The convergence of the multi-layer tree, the number of layers, and node are shown in Figure 6.

E. Quantum flux

In the case of classical MD simulations, the initial kinetic energy of the projectile has a sharp value. This allows to directly extract the energy distribution of scattered H atoms as a function of the incidence energy to compare with experimental results. In contrast, in the quantum case, the initial kinetic energy of a wavepacket is represented by a broad distribution, which means that additional analysis of the scattered wavepacket is necessary. This task can be achieved by evaluating the quantum flux^{21,41}.

The quantum flux can be measured by analyzing the part of the wavefunction which is absorbed by a complex absorption potential (CAP)^{42,43}. The main task of the CAP is to prevent the reflection of the wavefunction from the end points of the grid. Luckily, the CAP can also be used as an analysis tool. In our QD simulations, the CAP is activated after the H atom reaches the surface and starts to work at the distance of $Z_c = 6$ Bohr above the graphene.

A flux correlation function is computed from CAP matrix elements with respect to the time-dependent wavefunction. A Fourier transform of this correlation function yields the

energy-resolved flux, which in the time-independent picture has the following form²¹:

$$F(E) = 2\pi \langle \Psi_0 | \delta(H - E) \hat{F} \delta(H - E) | \Psi_0 \rangle, \quad (16)$$

where $\Psi_0 = \Psi(t=0)$ is the initial state and

$$\hat{F} = i[H, \Theta] \quad (17)$$

is the quantum flux operator. Here Θ is a Heaviside step function, which is non-zero in the region where the CAP works, *i.e.*, for $Z > Z_c$. Therefore, the flux operator \hat{F} measures the quantum flux through a hyperplane defined by equation $Z = Z_c$. Despite the energy E in Eq. (16) is the total energy of the system, it deviates from the initial kinetic energy of the H atom only by a constant, since the graphene surface is initially in an eigenstate (the ground state). With that we obtain the incidence energy resolved information for H atom scattering from the QD simulations. It is noteworthy that Eq. (16) is useful for evaluating sticking probabilities $S(E) = 1 - F(E)/|\Delta E|^2$, where

$$\begin{aligned} |\Delta E|^2 &= \langle \Psi_0 | \delta(H - E) | \Psi_0 \rangle \\ &= \frac{1}{\pi} \text{Re} \int_0^\infty e^{iEt} \langle \Psi_0 | \Psi(t) \rangle dt \end{aligned} \quad (18)$$

is the energy density function.

In order to extract the final kinetic energy distribution of the H atoms, the final kinetic energy resolved flux is to be determined. To this end we introduce an operated flux operator

$$\hat{F}_O = \frac{1}{2} (\hat{F} \hat{O} + \hat{O} \hat{F}), \quad (19)$$

where the Hermitian operator \hat{O} is here chosen as a projector onto a momentum state $|p\rangle$ of the H atom.

$$\hat{O} = |p\rangle \langle p| \quad (20)$$

The desired energy-resolved flux is obtained by substituting the operator \hat{F} in Eq. (16) with \hat{F}_O defined by Eq. (19), where p is p_X , p_Y , or p_Z . The transformation from momenta to the corresponding kinetic energies is straightforward.

As we work with grids of finite length, the momentum is discretized and its eigenfunctions read

$$\langle x | p_n \rangle = L^{-1/2} \exp(ik_n x), \quad (21)$$

where L is the length of the grid, $k_n = 2n\pi/L$ with $-N/2 < n < N/2$, and N is the number of grid points (we use the equidistant FFT grid). The momentum resolution is thus limited by the length of the grid. Note that the Z -grid in Z direction is longer than the X - and Y -grids.

To determine the resolution of the projectors we performed a 3D QD simulation with graphene DoFs fixed. The H atom was sent to the rigid graphene surface along the normal with the incidence energy $E = 1.96$ eV. The initial wavefunction in X - and Y -directions was set to be a constant while accounting for periodic boundary conditions. We expect the outgoing kinetic energy of the H atom to be equal to its initial kinetic energy, since the collision with the rigid surface has to be elastic.

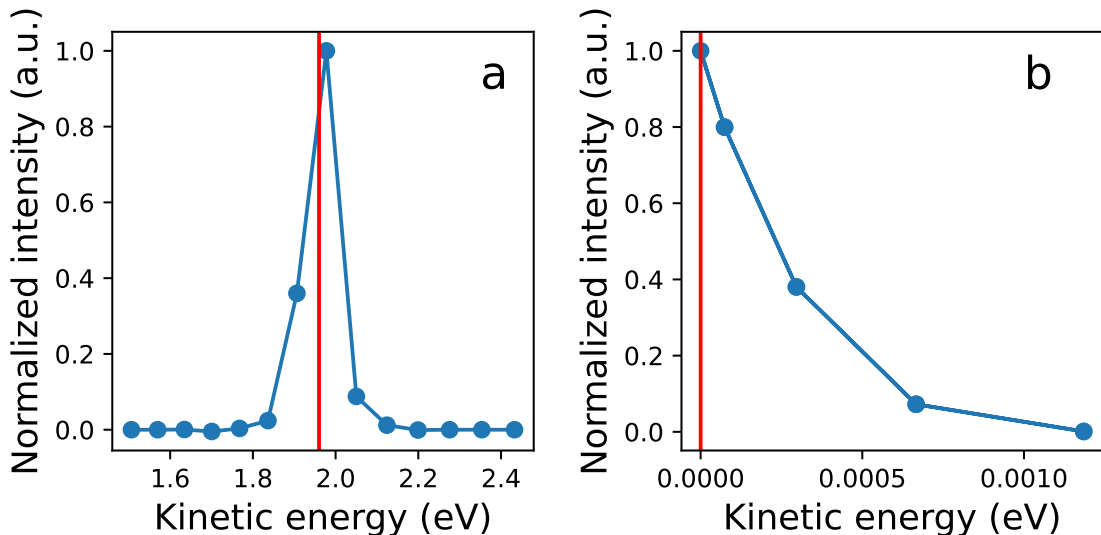


FIG. 7. The H atom outgoing kinetic energy distributions along (a) Z direction and (b) X direction (blue connected circles) calculated with 3D MCTDH simulations. The initial kinetic energy of the H atom is indicated by the red vertical lines.

The resolution of the projectors is demonstrated in Figure 7. As expected, the outgoing kinetic energy has some width due to the final grid length, as discussed above, producing the momentum resolution $\Delta p = \frac{2\pi}{L}$. Plots in Figure 7 indicate that the resolution is good enough for the following theoretical studies of H scattering from graphene.

F. cMD simulations details

Unlike the QD simulation, in which the wavefunction is propagated, in the cMD simulation, each atom is considered as a particle that obeys the Newton equations. We need to perform several thousands of different trajectories calculations to have statistically converged results. As mentioned, the initial condition for the C-atoms is prepared by a relaxation calculation, which means that the slab temperature is equal to 0 K. However, in a full classical molecular dynamic simulation, 0 K means the C-atoms are at their equilibrium position, and there is only one geometry. The result of the corresponding simulation leads to very different results from the QD simulations. In order to have comparable results with the QD simulations, the cMD initial conditions should be as similar as possible to those of the QD simulation. We thus introduce a "quantum mechanical character" in the cMD initial condition for the Carbon atoms to mimic the vibrational ground state of the graphene surface.

We generated 20 000 cMD trajectories simulating H atom scattering from graphene. The initial positions and momenta of H atoms were sampled from the time-reversed propagation of the distribution obtained from the hydrogen wavefunction when it reaches the graphene surface in QD simulation. Since graphene is initially in the vibrational ground state, we applied the following procedure to mimic this in the cMD simulations. For each normal mode of graphene n we generated a half-Gaussian distribution in the energy domain E_n with the average equal to the ground state energy $\frac{1}{2}\omega_n$. Then coordinates q_n and momenta p_n of the normal mode n were sampled as

$$q_n = \sqrt{2E_n/\omega_n} \cos \theta, \quad p_n = \sqrt{2mE_n} \sin \theta, \quad (22)$$

where angles θ were picked up from the uniform distribution from 0 to 2π . Finally, We transformed the distributions for normal coordinates and momenta into Cartesian coordinates using Eq. (1).

We generated 1000 graphene initial states using the above procedure. The corresponding average total energy is 0.697 eV, which agrees with the ground state energy 0.710 eV of graphene calculated from the MCTDH. The small discrepancy is due to the harmonic approximation used to produce the distributions Eq. (22). Figure 8 compares the histogram of the classical sampling and the wavefunction in QD simulation for the normal coordinate q_1 and momentum p_1 . They show very good agreement.

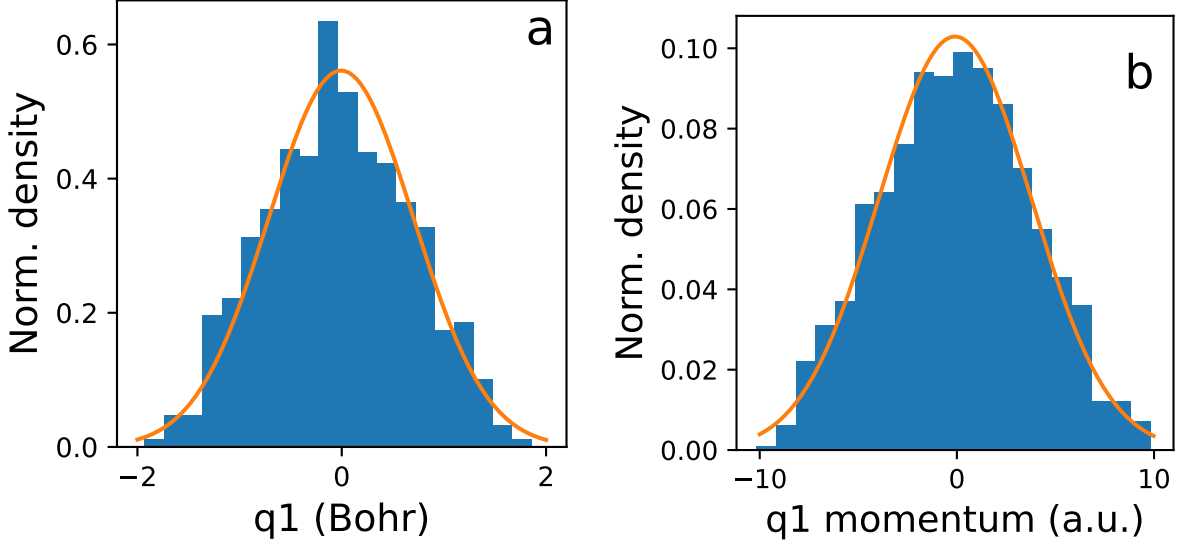


FIG. 8. The classical sampling histogram distribution (blue bars) and the MCTDH initial wavefunction density (orange curve) for (a) normal coordinate q_1 and (b) normal momentum p_1 .

Thus, we produced the cMD initial conditions for H atom and graphene as close as possible to those of the QD simulation, which will allow us to compare their outcomes.

III. RESULTS AND DISCUSSION

A. Energy transfer

We calculated the expectation values of total energies for each normal mode during the collision in the QD simulation and, similarly the average values of trajectories in the cMD simulations for the H atom scattering with the initial kinetic energy of 1.96 eV.

The plots in Figure 9 illustrate the expectation value of the total energy in electron volts (eV). This total energy is the sum of kinetic energy and potential energy. To compute the potential energy, we use the approximation harmonic and calculate the expectation value of the position of the normal mode. Additionally, we subtract the zero-point energy (ZPE) for each normal mode during the collision. The dashed black lines represent the distance between the hydrogen (H) atom and the graphene surface in Bohr units.

The QD and cMD simulations yield similar results. Before the hydrogen atom reaches its closest position, the energies of the normal modes q_{10} and q_4 increase. This behavior

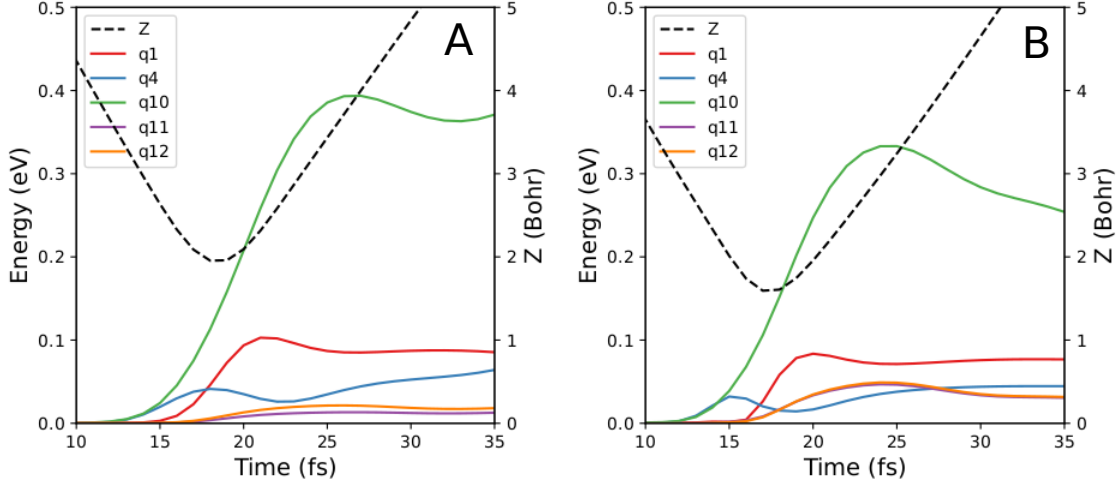


FIG. 9. For the QD simulation (a) and the cMD simulation (b), average values of the total energy for some normal modes of the graphene surface during the collision minus their ZPE for 15D simulation with the initial kinetic energy of 1.96 eV. All other normal modes not shown in the figure have energy smaller than 0.02 eV. The dashed black curves are the distance between the H atom and the graphene surface, see the y-axis on the right.

indicates an attempt to capture the approaching H atom and form a C-H chemical bond. Once the H atom reaches its minimum distance, a rapid heating process occurs between the H atom and the carbon (C) atom. Consequently, the energy of mode q_4 decreases, while the energy of mode q_1 increases.

However, there are slight discrepancies between the QD and cMD simulations. In the QD simulations, mode q_{10} absorbs more energy compared to the cMD simulation. On the other hand, in the cMD simulation, modes q_{11} and q_{12} absorb more energy. This difference might arise due to the less accurate description of the decoupling of normal modes in the MD method in which the Cartesian coordinates are used for the C atoms in the simulations.

B. Sticking probability

The sticking probabilities for all simulations are shown in the table III. The sticking probability calculated in the QD simulations and the cMD simulations are close for the initial kinetic energy of 1.96 eV : this probability is very small for this energy. However, there exists a larger difference between these two types of simulations for the initial kinetic

Conditions	H atom		D atom	
	1.96 eV	0.96 eV	1.96 eV	0.96 eV
cMD	0.1%	20%	0.9%	32%
QD	0.2%	29%	1.6%	39%

TABLE III. Sticking probability

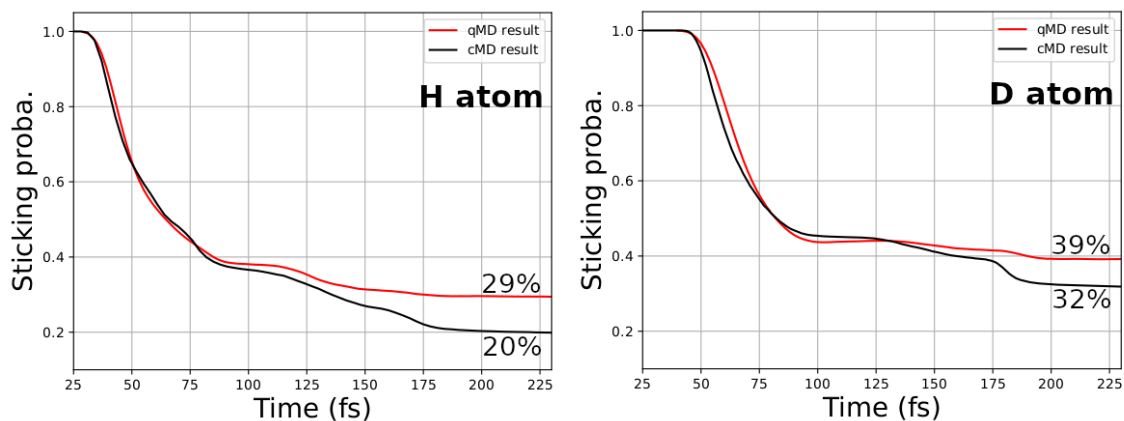


FIG. 10. Sticking probability after the collision for the initial kinetic energy of 0.96 eV for H atom (left) and D atom (right) in 15D simulations. The red curves are the results QD simulations the black curves are the results of cMD simulations.

energy of 0.96 eV, and the difference is smaller for the D atom than the H atom. This difference approves the enhancement of sticking probability by quantum effects, which shows an isotopic effect.

More details for the simulations with the initial kinetic energy of 0.96 eV are shown in figure 10. At the beginning of collision, all the projectile atoms are on the surface, thus the sticking probability decreases from 1. There are several plateaus before the sticking probability is stable and arrives at the minimum. The projectiles leave the surface wave after wave, as shown in figure 11. We observed the double nodes of the wave function in the Z direction of the H atom, which signifies the vibrational excited of the formed C-H chemical bound. The nodes of the wave function remain until 90 fs. Thus the quantum interference may explain this difference of sticking probability.

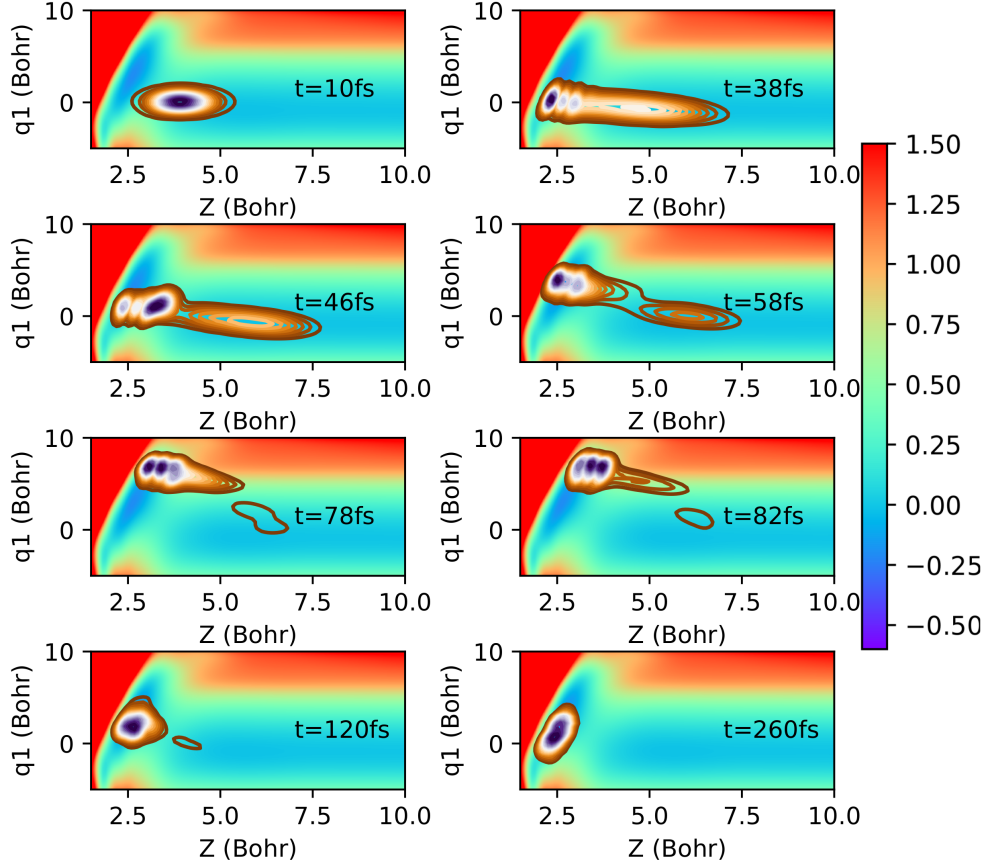


FIG. 11. The 2D reduced wave function density for the Z directions of the H atom (x-axis) and the q_1 normal mode (y-axis) at 10fs, 38fs, 46fs, 58fs, 78fs, 82fs, 120fs, and 260fs during the simulation on the PES 2D cut from the DOFs correspondent for the simulation of H atom with initial kinetic energy of 0.96 eV.

C. Scattering distribution

We studied the influence of collision at different positions of the graphene surface, figure 12 is the H atom outgoing kinetic energy distribution of attacking the center of C-C chemical bond and the center of carbon ring, Figure 13(A,C) is for attacking on the top of C atom. The H atom transfers the most energy to the graphene surface in the case of attacking the top and the least on the center of the ring. The collision of the H atom with the initial kinetic energy of 0.96 eV at the center of the ring is quasi-elastic. Closer to the top of the C atom, more energy is transferred.

In the simulations of attacking the center of the carbon ring, the sticking probability con-

sistently registers as zero, regardless of the varied initial kinetic energies. This is attributed to the absence of a chemisorption site at the central point of the ring. When directing the attack towards the center of the C-C bond with an initial kinetic energy of 1.96 eV , the sticking probability is found to be less than 0.1% in both cMD and QD simulations. However, when the initial kinetic energy is 0.96 eV , the cMD simulation yields a 12.5% sticking probability, while the QD simulation records a 15% sticking probability. This non-zero sticking probability arises from the close proximity of the chemical bond center to the C atom, facilitating diffusion and attachment of the H atom to form the C-H chemical bond. It's worth noting, however, that this probability remains lower than that observed when targeting the top of the C atom, where the H atom demonstrates a higher probability of forming a C-H chemical bond.

We studied the case of attacking the top of the C atom in more depth. Figure 14 depicts the scattering distribution for the H atom and the D atom in the QD and cMD calculations, respectively. Their results are coherent. The D atom transfers more energy to the graphene surface than the H atom, because with the same initial kinetic energy, the velocity of the D atom is smaller than that of the H atom, and the D atom has more time to interact with the C atoms and then transfers more energy to the C atoms.

D. Full dimensional simulation

We performed a full dimensional simulation (75D) for a H atom with 1.96 eV initial kinetic energy and incident angle of 0° . There is not much difference between QD and cMD simulations. We calculated the kinetic energy of C atoms during the collision as figure 15. Both QD and cMD simulations can observe the energy transfer from the center C atom and first shell C atoms to the second shell C atoms. The center C atom received more energy in the Z direction than the XY plane, while the second shell C atoms received more energy in the XY plane than in the Z direction.

We calculated also the H atom outgoing kinetic energy distribution (figure 17) and the 2D scattering diagram (figure 16), and there are not many differences from the calculation of 15D.

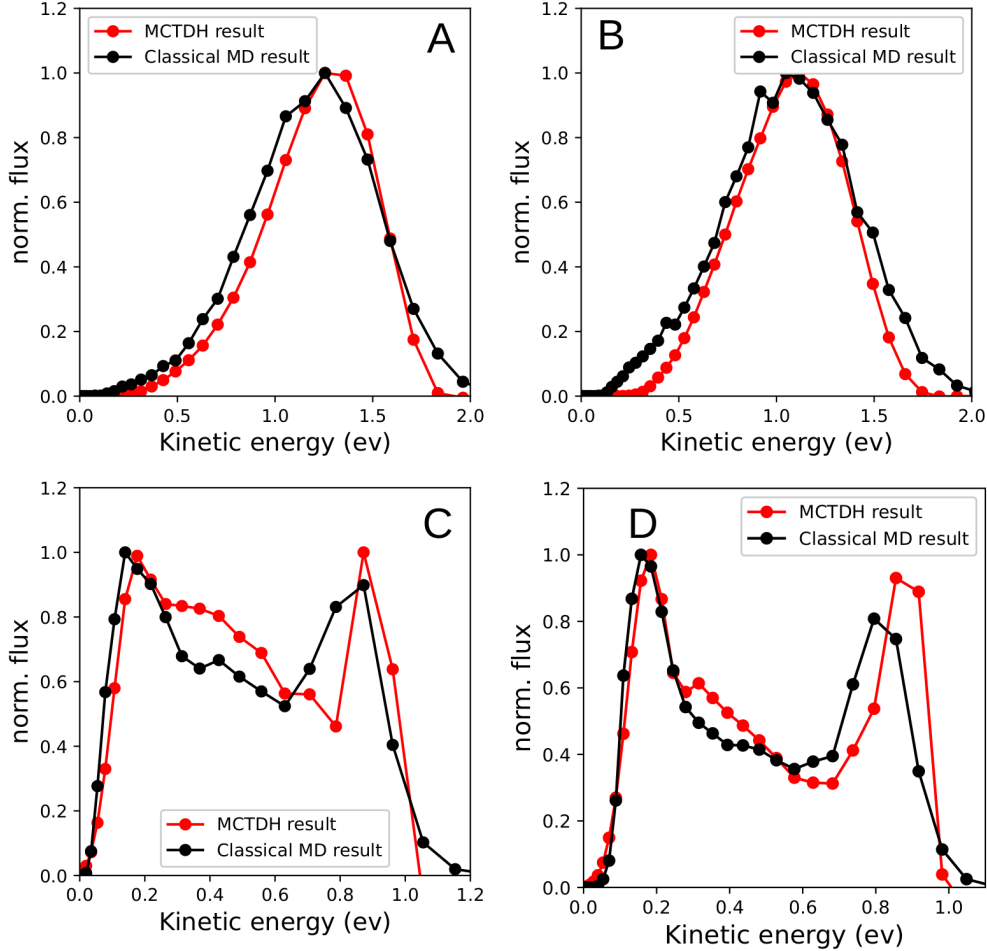


FIG. 12. Outgoing kinetic energy distribution for H atom with initial kinetic energy of 1.96 eV (A and B) and of 0.96 eV (C and D) attacking the center of C-C chemical bond (A and C) and then the center of the carbon ring (B and D) in the MCTDH calculations (red curves) and the cMD calculations (black curves) for 15D simulations.

IV. CONCLUSION

In this work, we performed cMD and QD simulations under comparable initial conditions and with incident energies of 1.96 and 0.96 eV and an incident angle of 0° . By comparing the results of the two simulations, we found that they are well coherent for both the H atom and the D atom especially for 1.96 eV, indicating that there is no evidence of a strong quantum effect in these collision conditions. This is likely due to the fact that the incident energy of 1.96 eV is high, which means that the system is in the classical regime where quantum effects are less pronounced. A close look at the results show some differences especially at 0.96 eV.

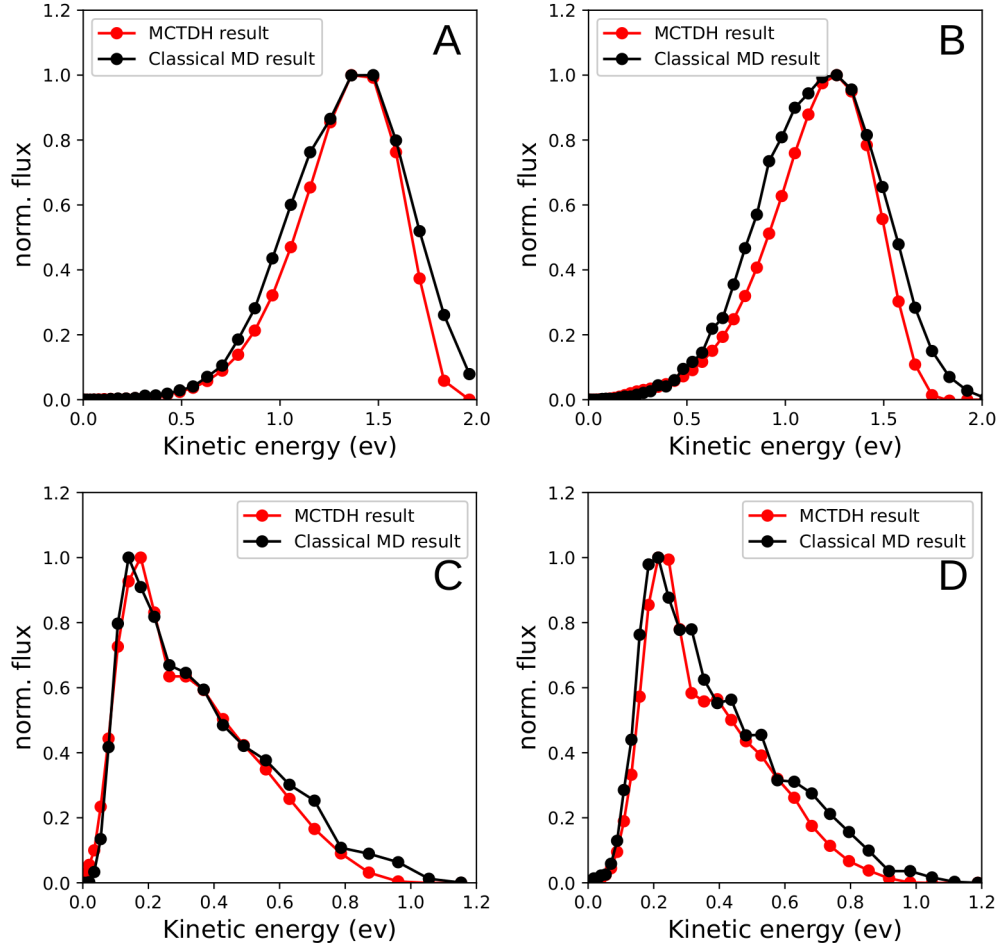


FIG. 13. Outgoing kinetic energy distribution for the H atom (A and C) and the D atom (B and D) with the initial kinetic energy of 1.96 eV (A and B) and 0.96 eV (C and D) for cMD simulations (black curves) and for QD simulations (red curves) for 15D simulations.

The agreement between the results of the cMD and QD simulations also supports the validity of the methods used in the QD simulations for which we developed new numerical tools such as projectors along the different Cartesian directions. Thus, we can use those methods in the following full-dimensional simulations. In particular, it will be possible to start with a wave plane with all the degrees of freedom, the cell being considered as periodic. This will allow us to directly compare with experimental results, since one can then define easily the incident angle and the hydrogen atoms can reach all the parts of the surface. The possibility to treat such large systems is new and is possible thanks to the development of ML-MCTDH and more recently of the MCCPD method.

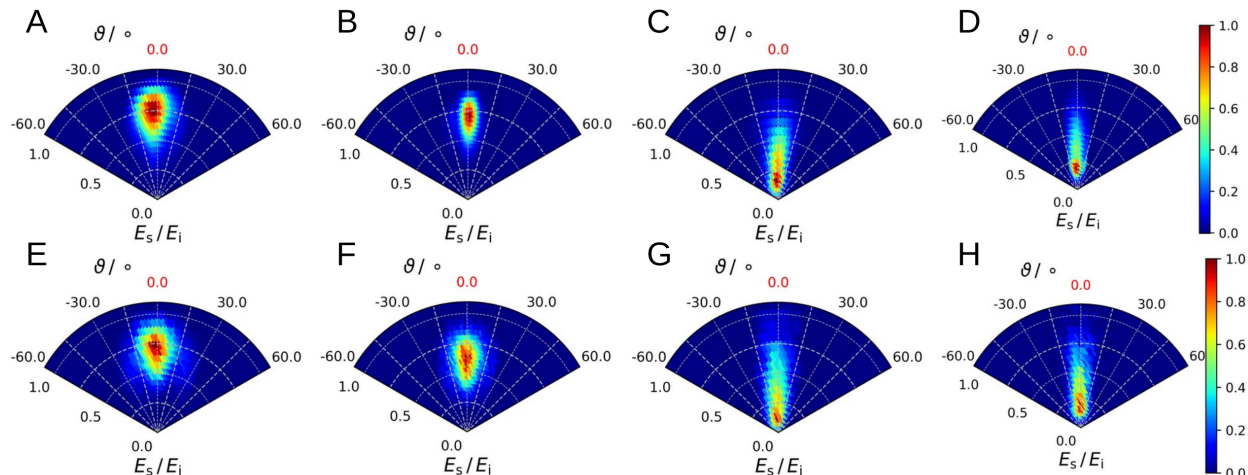


FIG. 14. 2D scattering distribution diagrams for QD simulations (A, B, C, D) and for cMD simulations (E, F, G, H) for the H atom (A, C, E, G) and the D atom (B, D, F, H) with the initial kinetic energy of 1.96 eV (A, B, E, F) and 0.96 eV (C, D, G, H) for 15D simulations.

V. ACKNOWLEDGEMENT

The authors thank the computational platforms IDRIS HPE Jean Zay (project A0110812942) and Ruche Mesocentre and the CNRS International Research Network (IRN) “MCTDH” for financial support. A.K. acknowledges support from the European Research Council (ERC) under the European Union’s Horizon 2020 research and innovation programme (grant agreement no. 833404).

REFERENCES

- ¹P. R. Wallace, Phys. Rev. **71**, 622 (1947).
- ²K. S. Novoselov, A. K. Geim, S. V. Morozov, D. Jiang, Y. Zhang, S. V. Dubonos, I. V. Grigorieva, and A. A. Firsov, Science **306**, 666 (2004).
- ³C. Fang, J. Zhang, X. Chen, and G. J. Weng, Nanomaterials **10**, 1 (2020).
- ⁴K. Burnett, P. S. Julienne, P. D. Lett, E. Tiesinga, C. J. Williams, H. L. Bethlem, G. Berden, A. J. A. van Roij, L. Hornekaer, A. Baurichter, V. V. Petrunin, D. Field, and A. C. Luntz, Adv. Atom. Mol. Opt. Phys **71**, 6455 (1999).
- ⁵K. S. Novoselov, V. I. Fal’Ko, L. Colombo, P. R. Gellert, M. G. Schwab, and K. Kim, Nature **490**, 192 (2012).

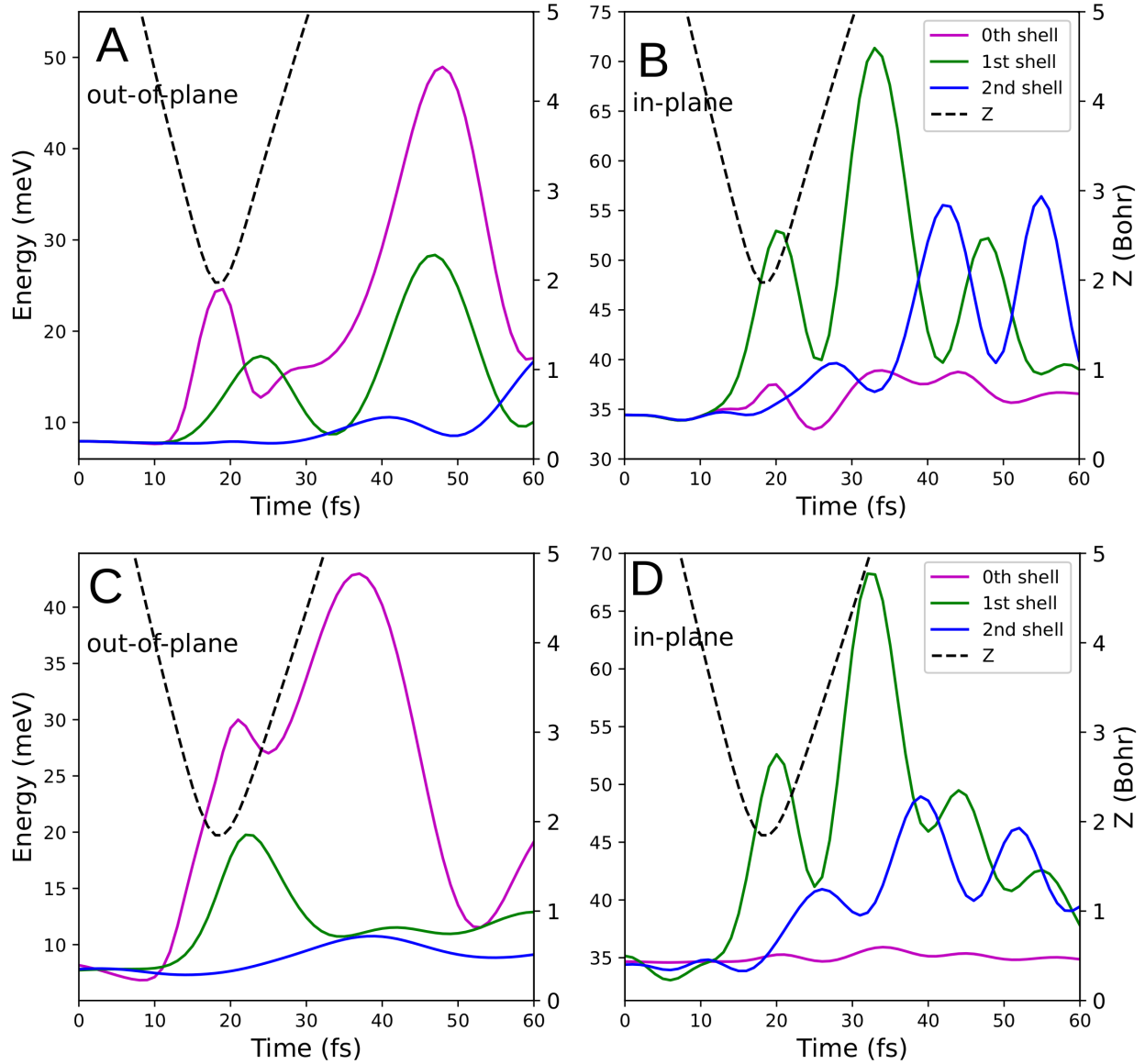


FIG. 15. Kinetic energy per C atom during the collision for 75D QD simulation (A and B) and cMD simulation (C and D) for the center C atom (purple curve), the first shell C atoms (green curve) and the second shell C atoms (blue curve) in the Z direction (A and C, out-of-plane) and in the XY plane (B and D, in-plane). The z-coordinate of the H-atom (ordinate on the left-hand side) is indicated by the dashed black curve.

⁶L. Schlapbach and A. Züttel, “Hydrogen-storage materials for mobile applications,” in *Materials for Sustainable Energy* (World Scientific, 2001) pp. 265–270.

⁷S. P. Lonkar, Y. S. Deshmukh, and A. A. Abdala, *Nano Research* **8**, 1039 (2015).

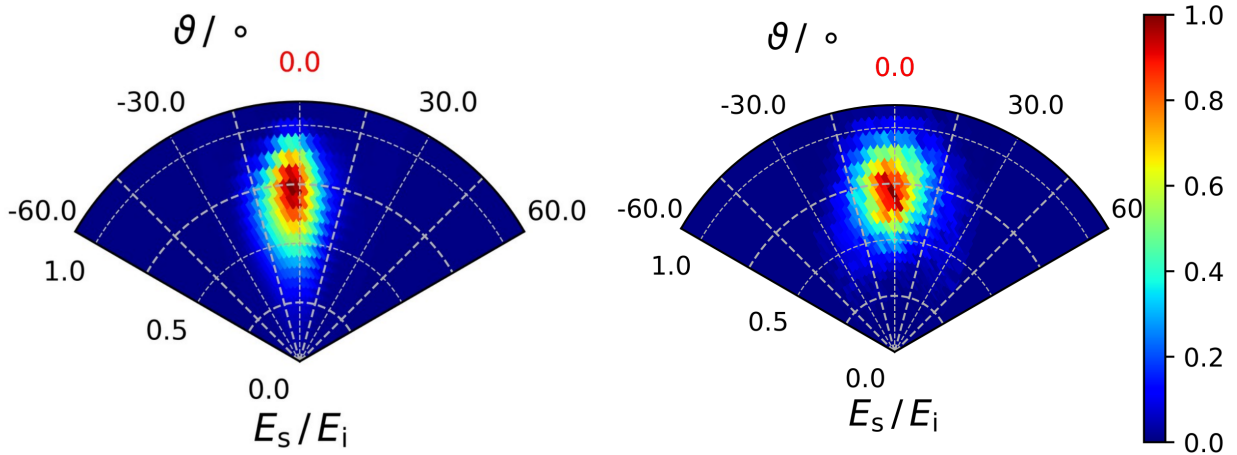


FIG. 16. 2D scattering distribution for QD simulation (left) and cMD simulation (right) for 75D simulations with initial kinetic energy of 1.96 eV.

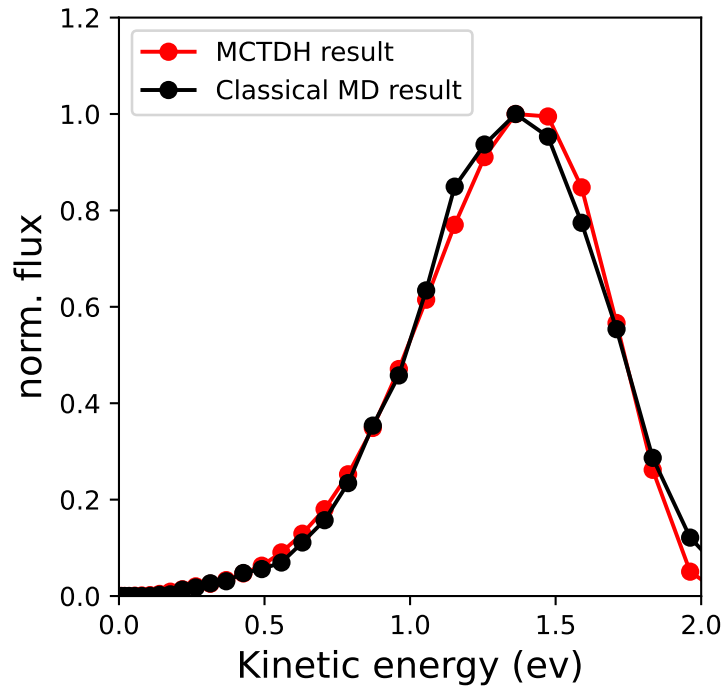


FIG. 17. Outgoing kinetic energy distribution for the H atom in cMD simulation (black curve) and QD simulation (red curve) for 75D simulations with initial kinetic energy of 1.96 eV.

⁸R. Balog, B. Jørgensen, L. Nilsson, M. Andersen, E. Rienks, M. Bianchi, M. Fanetti, E. Lægsgaard, A. Baraldi, S. Lizzit, Z. Sljivancanin, F. Besenbacher, B. Hammer, T. G. Pedersen, P. Hofmann, and L. Hornekær, Nature Materials **9**, 315 (2010).

- ⁹H. Jiang, M. Kammler, F. Ding, Y. Dorenkamp, F. R. Manby, A. M. Wodtke, T. F. Miller, A. Kandratsenka, and O. Bünermann, *Science* **364**, 379 (2019).
- ¹⁰M. Bonfanti, S. Achilli, and R. Martinazzo, *Journal of Physics: Condensed Matter* **30**, 283002 (2018).
- ¹¹K. Spyrou, D. Gournis, and P. Rudolf, *ECS Journal of Solid State Science and Technology* **2**, M3160 (2013).
- ¹²S. Wille, H. Jiang, O. Bünermann, A. M. Wodtke, J. Behler, and A. Kandratsenka, *Physical Chemistry Chemical Physics* **22**, 26113 (2020).
- ¹³J. Behler and M. Parrinello, *Phys. Rev. Lett.* **98**, 146401 (2007).
- ¹⁴H. Jiang, X. Tao, M. Kammler, F. Ding, A. M. Wodtke, A. Kandratsenka, T. F. Miller, and O. Bünermann, *Journal of Physical Chemistry Letters* **12**, 1991 (2021).
- ¹⁵H.-D. Meyer, U. Manthe, and L. S. Cederbaum, *Chem. Phys. Lett.* **165**, 73 (1990).
- ¹⁶U. Manthe, H.-D. Meyer, and L. S. Cederbaum, *J. Chem. Phys.* **97**, 3199 (1992).
- ¹⁷M. H. Beck, A. Jäckle, G. A. Worth, and H.-D. Meyer, *Phys. Rev.* **324**, 1 (2000).
- ¹⁸H.-D. Meyer and G. A. Worth, *Theor. Chem. Acc.* **109**, 251 (2003).
- ¹⁹H.-D. Meyer, F. Gatti, and G. A. Worth, eds., *Multidimensional Quantum Dynamics: MCTDH Theory and Applications* (Wiley-VCH, Weinheim, 2009).
- ²⁰H.-D. Meyer, *Wiley Interdisciplinary Reviews: Computational Molecular Science* **2**, 351 (2012).
- ²¹F. Gatti, B. Lasorne, H.-D. Meyer, and A. Nauts, *Applications of Quantum Dynamics in Chemistry*, Vol. 98 (in: *Lectures Notes in Chemistry*, Springer, Heidelberg, 2017).
- ²²A. Jäckle and H. D. Meyer, *Journal of Chemical Physics* **104**, 7974 (1996).
- ²³A. Jäckle and H. D. Meyer, *Journal of Chemical Physics* **109**, 3772 (1998).
- ²⁴D. Peláez and H.-D. Meyer, *J. Chem. Phys.* **138**, 014108 (2013).
- ²⁵R. L. Panadés-Barrueta and D. Peláez, *J. Chem. Phys.* **153**, 234110 (2020).
- ²⁶Q. Song, X. Zhang, D. Peláez, and Q. Meng, *J. Phys. Chem. Lett.* **13**, 11128 (2022).
- ²⁷U. Manthe, *J. Chem. Phys.* **105**, 6989 (1996).
- ²⁸R. van Harrevelt and U. Manthe, *J. Chem. Phys.* **123**, 064106 (2005).
- ²⁹R. Ellerbrock and U. Manthe, *J. Chem. Phys.* **156**, 134107 (2022).
- ³⁰M. Schröder, *Journal of Chemical Physics* **152** (2020), 10.1063/1.5140085.
- ³¹H. Wang and M. Thoss, *Journal of Chemical Physics* **119**, 1289 (2003).
- ³²U. Manthe, *J. Chem. Phys.* **128**, 164116 (2008).

- ³³O. Vendrell and H.-D. Meyer, *Journal of Chemical Physics* **134** (2011), 10.1063/1.3535541.
- ³⁴G. A. Worth, M. H. Beck, A. Jäckle, O. Vendrell, and H.-D. Meyer, The MCTDH Package, Version 8.2, (2000). H.-D. Meyer, Version 8.3 (2002), Version 8.4 (2007). O. Vendrell and H.-D. Meyer Version 8.5 (2013). H.-D. Meyer, Version 8.6 (2021). Versions 8.5 and 8.6 contain the ML-MCTDH algorithm. Used versions: 8.6.3 (Jan 2023). See <http://mctdh.uni-hd.de/>.
- ³⁵D. J. Auerbach, S. M. Janke, M. Kammler, A. Kandratsenka, and S. Wille, “Molecular dynamics tian xia 2 (mdt2); program for simulating the scattering of atoms and molecules from a surface (github repository). available at https://github.com/akandra/md_tian2,” (2020).
- ³⁶G. Pasin, F. Gatti, C. Iung, and H. D. Meyer, *Journal of Chemical Physics* **124** (2006), 10.1063/1.2192499.
- ³⁷M. Schröder, F. Gatti, D. Lauvergnat, H.-D. Meyer, and O. Vendrell, *Nat. Comm.* **13**, 6170 (2022).
- ³⁸I. Kosztin, B. Faber, and K. Schulten, *American Journal of Physics* **64**, 633 (1996).
- ³⁹H.-D. Meyer, F. Le Quéré, C. Léonard, and F. Gatti, *Chemical Physics* **329**, 179 (2006).
- ⁴⁰D. J. Tannor, *Introduction to Quantum Mechanics: A Time-Dependent Perspective* (University Science Books, 2007).
- ⁴¹A. Jäckle and H.-D. Meyer, *J. Chem. Phys.* **102**, 5605 (1995).
- ⁴²U. V. Riss and H.-D. Meyer, *J. Phys. B* **26**, 4503 (1993).
- ⁴³U. V. Riss and H.-D. Meyer, *J. Chem. Phys.* **105**, 1409 (1996).